J. Fluid Mech. (1979), *vol.* 91, *part* 1, *pp.* 1–16
Printed in Great Britain

Evaluation of subgrid-scale models using an accurately simulated turbulent flow

By ROBERT A. CLARK
Group TD-5, Los Alamos Scientific Laboratory, Los Alamos, New Mexico 87544
JOEL H. FERZIGER AND W. C. REYNOLDS
Department of Mechanical Engineering, Stanford University, Stanford, California 94305

(Received 14 March 1978 and in revised form 19 June 1978)

We use a calculation of periodic homogeneous isotropic turbulence to simulate the experimental decay of grid turbulence. The calculation is found to match the experiment in a number of important aspects and the computed flow field is then treated as a realization of a physical turbulent flow. From this flow, we compute the large eddy field and the various averages of the subgrid-scale turbulence that occur in the large eddy simulation equations. These quantities are compared with the predictions of the models that are usually applied in large eddy simulation. The results show that the terms which involve the large-scale field are accurately modelled but the subgrid-scale Reynolds stresses are only moderately well modelled. It is also possible to use the method to predict the constants of the models without reference to experiment. Attempts to find improved models have not met with success.

1. Introduction

It is not possible to calculate most turbulent flows in complete detail because the range of length scales is so large that the amount of data that would have to be handled is orders of magnitude greater than the capacity of any existing or projected computer. For this reason, the traditional approaches to computing turbulent flows have been based on O. Reynolds' idea of averaging the Navier–Stokes equations over an ensemble of flows or over an appropriate interval of time or space. One then has equations for an averaged velocity field $\overline{u}(x,t)$, where the overbar denotes averaging according to the definition employed. If we then define a fluctuating velocity component by $u(x,t) = \overline{u}(x,t) + u'(x,t)$, the averaged equations can be written (for an incompressible flow with constant viscosity)

$$\frac{\partial \overline{u}_i}{\partial t} + \frac{\partial}{\partial x_j}\overline{u}_i\overline{u}_j = -\frac{\partial \overline{p}}{\partial x_i} + \nu\nabla^2\overline{u}_i - \frac{\partial}{\partial x_j}R_{ij}, \tag{1}$$

$$\partial \overline{u}_i/\partial x_i = 0, \tag{2}$$

$$R_{ij} = \overline{u_i'u_j'} \tag{3}$$

since $\overline{\overline{u}}_i = \overline{u}_i$ and $u_i' = 0$ as a consequence of the definition of averaging. To close this system of equations, it is necessary to find an expression for R_{ij} (the Reynolds stress) in terms of $\overline{u}_i$.

0022-1120/79/4207-6000 $02.00

In large eddy simulation, one averages the Navier–Stokes equations over a small spatial region in order to remove the small-scale fluctuations. The resulting equation for the large-scale field contains a term similar to, but more complicated than, the Reynolds stress R_{ij} of (1) and (3) and this term (the *subgrid-scale* Reynolds stress) must be modelled. These operations are discussed in § 3.

Several models for the subgrid scale R_{ij} have been proposed. The problem has been to verify a proposed model. The best that could be done until now was to compare the evolution of the computed large-scale structures with those in an experiment (see, for example, Deardorff 1970; Mansour *et al.* 1977). This will not reveal whether the actual subgrid-scale Reynolds stress is being accurately modelled, but only whether the subgrid-scale Reynolds stress and the model have the same net effect on the statistics of the large-scale motions for the particular flow in question. In addition, virtually all models contain at least one adjustable constant which must be set by some theoretical argument or selected to fit some important aspect of an experiment. On the other hand, if there were an experiment which measured everything from the largest turbulent structure to the smallest eddy, it would then be possible to compute the subgrid-scale R_{ij} exactly, and compare its value at each point in space with the prediction of a model. Unfortunately, no laboratory experiment is capable of such measurements.

In place of a laboratory experiment, we have numerically calculated a three-dimensional turbulent flow field on a fine grid (64 grid points on a side) by directly integrating the Navier–Stokes equations without having to average the equations. We have used the result to examine subgrid-scale models on a coarse mesh overlayed on the original fine mesh. Practical limitations require that this be done at a relatively low Reynolds number, since at high Reynolds numbers the difference in scale between the largest and smallest eddies renders computer simulation impractical. Despite this, we shall see that the computed case is relevant to important flows.

In § 2 we describe how the calculation of the turbulent flow field was done and cite some results which indicate that we do have an accurate representation of a truly turbulent flow. In § 3 we give the results of comparisons between models for the subgrid-scale quantities and the 'exact' values obtained from our 'experimental' flow field.

2. Simulation of isotropic turbulence

Because this is a first attempt at model verification, we chose the simplest possible flow field; homogeneous isotropic turbulence. Experimentally, this flow is approximated by grid turbulence produced by passing a uniform stream of fluid through a mesh. The decay is observed as the fluid proceeds downstream. Special care is necessary to assure isotropy; the most recent and careful such experiment is that of Comte-Bellot & Corrsin (1971), which we shall use as the base experiment.

To simulate grid turbulence we shall use the Navier–Stokes equations together with the continuity equation for an incompressible fluid:

$$\frac{\partial u_i}{\partial t} = -\frac{\partial}{\partial x_j}(u_i u_j) - \frac{\partial p}{\partial x_i} + \nu \nabla^2 u_i, \tag{4}$$

$$\partial u_i / \partial x_i = 0, \tag{5}$$

where we use the summation convention. We shall attempt to simulate the grid-turbulence experiment computationally by selecting a cube of fluid and following its history as it passes downstream from the grid. In order to do this successfully, we must assure that the cube we select is large enough that all correlations are essentially zero at distances equal to the side of the box. From a practical point of view, this means that the box must be large compared with the integral scale of the turbulence; the box should also be small enough that, under the conditions of the experiment, no significant changes in important integral properties occur over a distance equal to the size of the computational cube. If these conditions are met (and they are in the case under consideration), we may simulate the experiment by following the time history of the cube of fluid using periodic boundary conditions in all three spatial dimensions.

Equation (5) can be replaced by an equation for the pressure p. We apply the divergence operator to (4) and we are then left with a Poisson equation for the pressure:

$$\nabla^2 p = -\frac{\partial u_j}{\partial x_i}\frac{\partial u_i}{\partial x_j}. \tag{6}$$

In general terms, the method of solution is to start with the velocity field at time $n\delta t$, solve (6) for the pressure field at time $n\delta t$, then use (4) to find $\partial u_i/\partial t$ at $n\delta t$ and advance the solution to time $(n+1)\,\delta t$. Thus we ensure continuity at time $(n+1)\,\delta t$ by properly choosing the pressure at time $n\delta t$. This is a fairly standard numerical algorithm.

All special derivatives were calculated using fourth-order, space-centred, finite-difference approximations; the differencing of the convective term is both momentum and energy conserving, cf. Kwak, Reynolds & Ferziger (1975). Periodic boundary conditions were imposed and the three-dimensional Poisson equation for pressure was solved with the aid of fast Fourier transforms. The time-differencing scheme is a third-order-accurate predictor–corrector method. The predictor step is of leap-frog type,

$$(u^*)^{n+1} = u^{n-1} + 2\delta t(u^*)_t^n, \tag{7}$$

and the corrector step is

$$u^{n+1} = u^n + \tfrac{2}{3}\delta t(u^*)_t^n + \tfrac{5}{12}\delta t(u^*)_t^{n+1} - \tfrac{1}{12}\delta t(u^*)_t^{n-1}, \tag{8}$$

which will be recognized as an implicit Adams–Moulton method.

The main advantage of this third-order scheme is that only one time derivative, namely $(u^*)_t^{n+1}$, must be calculated at each time step. Since the computation of u_t requires the evaluation of the right-hand side of (4), virtually all of the computational effort is involved in calculating the time derivative of the velocity field (in which we include solving the associated Poisson equation for pressure), this method is only slightly slower than an explicit first-order scheme or the second-order leap-frog scheme. The third-order accuracy is obtained by saving the time derivatives of the velocity fields at times n and $n-1$. The stability criterion is similar to the standard Courant condition. Details of the method (which has not previously been used in this application) can be found in Clark, Ferziger & Reynolds (1977). An indication of this accuracy is given by figure 1, the results of a numerical test on the one-dimensional wave equation:

$$u_t + cu_x = 0. \tag{9}$$

u_x was calculated by the use of Fourier transforms so that the only error in the numerical solution is due to the time-differencing scheme. u was defined at 64 evenly

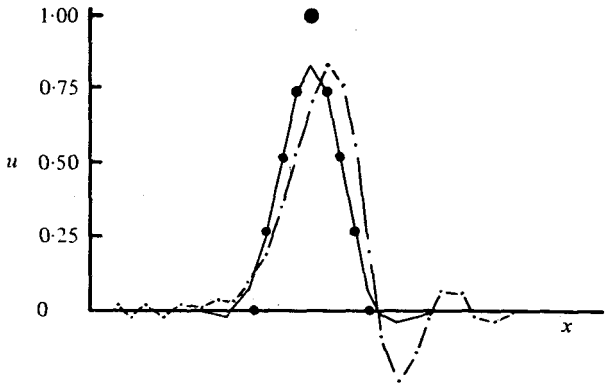

FIGURE 1. Solutions to $u_t + cu_x = 0$. ·—·—·, second order; ——, third order; ●, exact.

U_0T/M	$(U_1^2)^{\frac{1}{2}}$ (cm/s)	Dissipation rate (cm²/s³)	Kolmogorov microscale (cm)	Taylor microscale (cm)	R_λ $(U_1^2)^{\frac{1}{2}}\lambda/\nu$
240	6·75	145	0·069	0·845	38·1
385	5·03	48·5	0·091	1·09	36·6

TABLE 1. Gross properties of the turbulent flow. $U_0 = 10$ m/s, $M = 2{\cdot}54$ cm.

spaced points and was initially zero, except for the triangle shown hear the centre. Periodic boundary conditions were applied, and we set $c\delta t/\delta x = 0{\cdot}2$. In the exact solution, the triangle moves from left to right at the constant speed c, so that after 1600 time-steps the triangle should have swept across the grid five times and the exact solution is identical to the initial conditions. The third-order calculation used 3% more computing time than the leap-frog calculation and twice the amount of storage. It is clear that the third-order method is superior.

Comte-Bellot & Corrsin (1971) measured the downstream decay of grid-generated isotropic turbulence in a wind tunnel with free-stream velocity U_0. A time history was obtained by assuming that two points separated by a distance L in the flow direction are equivalent to the two times separated by $t = L/U_0$ in a flow with no mean velocity.

The conditions chosen for the simulation are given in table 1. U_0, the mean flow velocity, is 10 m/s, and M, the size of the mesh, is 2·54 cm. The initial conditions were set up to coincide with the experimental data at $U_0t/M = 240$. The initial conditions were given the same total energy and energy spectrum as the data and had zero divergence but were otherwise random.

The initial field does not represent true turbulence since it does not contain the local velocity correlations that exist in a physical field. It is these correlations which give rise to the subgrid-scale Reynolds stresses which we hope to model. We also note that the skewness, which is an indication of the presence of turbulence, is initially zero. The expectation is that, as the equations of motion are integrated in time, a representation of a true turbulent flow will develop.

Given the fixed number of mesh points in each direction, N, the physical size of the

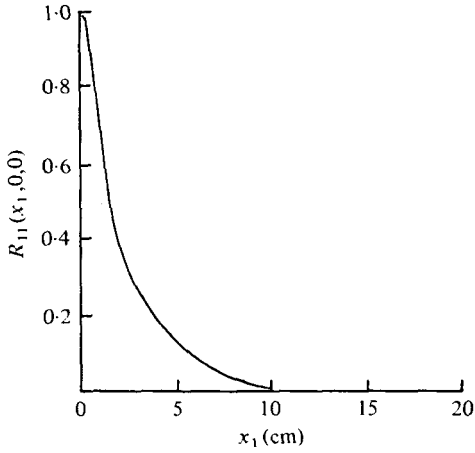

FIGURE 2. Velocity correlation function.

box of fluid, L, must be determined. The box must be large enough that the velocity correlation at $\frac{1}{2}L$ is negligible, and small enough that the highest wavenumber $k_{\max} = N\pi/L$ is large enough to include essentially all of the energy dissipation spectrum. The size of the box was chosen to be a cube of side 20 cm. Figure 2 gives the experimental velocity correlation function $R_{11}(r_1, 0, 0)$, where

$$R_{11}(r_1, 0, 0) = \frac{\rho_{11}(r_1, 0, 0)}{\rho_{11}(0, 0, 0)} \tag{10}$$

and

$$\rho_{11}(r_1, 0, 0) = \langle u_1(x_1 + r_1, x_2, x_3)\, u_1(x_1, x_2, x_3)\rangle.$$

We see that a 20 cm length is sufficient to meet the condition that the correlation at $\frac{1}{2}L$ be small. This choice also makes the mesh size small enough that most of the dissipation is contained in the resolvable scales. The time step was chosen to be 0·0073 s, which means that 50 time steps are required to go from $U_0 t/M = 240$, the initial state, to $U_0 t/M = 385$, the next experimental station.

In figure 3 we show the three-dimensional energy spectrum $E(k)$, the dissipation spectrum $D(k)$ and the energy transfer spectrum $T(k)$ of the final numerical flow field. $D(k)$ is simply $\nu k^2 E(k)$; $T(k)$ is calculated from

$$\partial E(k)/\partial t = T(k) + D(k); \tag{11}$$

$\partial E(k)/\partial t$ was calculated using the numerical values of u_i and $\partial(u_i^*)/\partial t$. The energy spectrum compares well with the experimental one. Comte-Bellot & Corrsin (1971), whose data we are attempting to match, did not compute $T(k)$. Van Atta & Chen (1969) have given $T(k)$ for a similar experiment. However, their spectrum is somewhat different from that of Comte-Bellot & Corrsin and we must expect that the transfer function $T(k)$ would also be different. We compared our results with Van Atta & Chen's and found that our results are somewhat shifted upward in wavenumber (which is consistent with the spectral differences) and the peak at low wavenumber is not as sharp. This is probably because we had to use fairly wide bandwidths to obtain good statistics.

We now examine some of the results. First, we consider the energy and its rate of

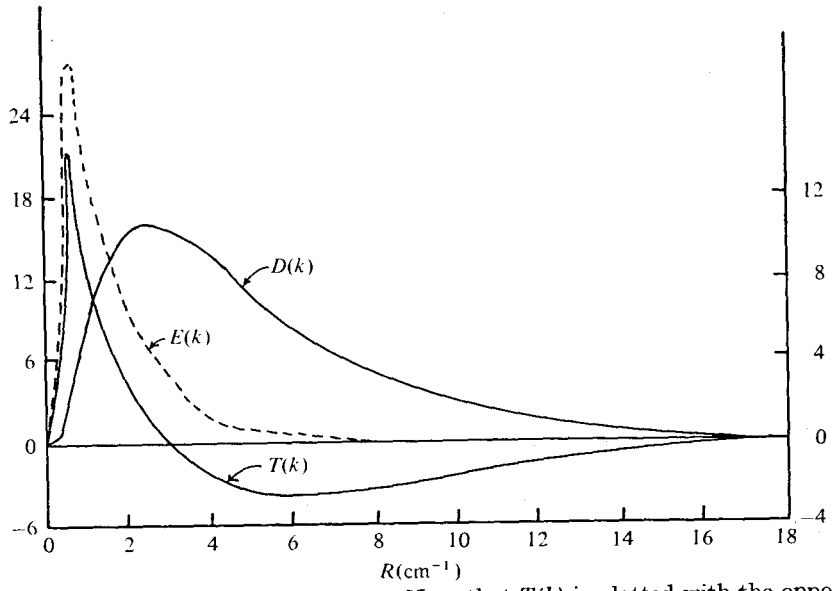

FIGURE 3. Energy transfer and dissipation. Note that $T(k)$ is plotted with the opposite sign.

change, the dissipation rate. The only source of dissipation is the physical viscosity $\nu = 0{\cdot}14$ cm^2 s^{-1}. If the simulation is accurate, its energy decay will match the experimental data; figure 4 demonstrates that this is the case. The mean energy in the numerical simulation at time-step 50 is only 3·2% lower than the experimental value. The dissipation rate, which is a more sensitive indicator, is 11·3% higher than the experimental value. This is apparently the result of too high a numerical transfer of energy from low to high wavenumbers; unfortunately, since Comte-Bellot & Corrsin did not measure $T(k)$, we cannot verify this directly.

The skewness of low Reynolds number wind-tunnel turbulence has been shown experimentally to be approximately 0·4 (Batchelor 1953). The skewness S is defined by

$$S = -\frac{\langle(\partial u_i/\partial x_i)^3\rangle}{\langle(\partial u_i/\partial x_i)^2\rangle^{\frac{3}{2}}} \quad \text{(no summation)}, \tag{12}$$

where $\langle\ \rangle$ indicates an ensemble average. The skewness of the numerical flow field, with the average taken over all grid points, is shown in figure 5. The skewness starts at zero, but after only 15 time steps it has stabilized at approximately the experimental value. The slight dip in the skewness which occurs at intervals of eight time steps is due to corrections which were made to eliminate an apparent weak instability in the time integration scheme. This is described further in Clark *et al.* (1977).

As the results seem to be in adequate agreement with the experimental data, we believe that the computed flow field may be accepted as a realization of an isotropic turbulent flow field and it will be used as such in the following section. Similar results could have been obtained by means of the Fourier methods employed by Orszag & Patterson (1972) and Rogallo (1977); the major difference between our calculation and theirs (other than the numerical method) is the initial conditions. We chose finite-difference methods mainly because they appear to be more easily extended to the inhomogeneous flows that we intend to study next.

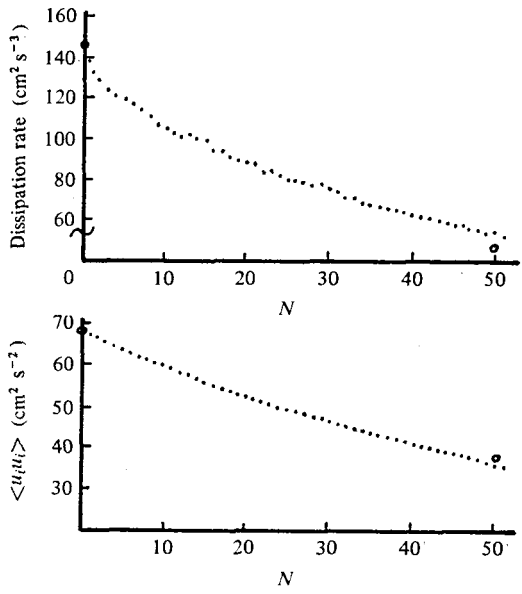

FIGURE 4. Dissipation rate and energy. ○, experiment; ●, calculated. $T = 0{\cdot}0073\,N$ s.

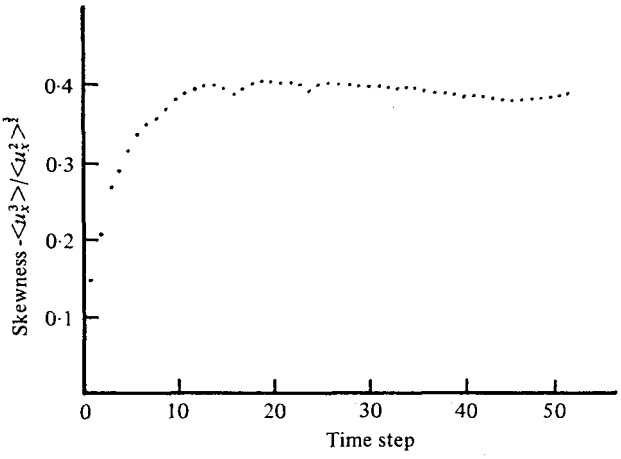

FIGURE 5. Skewness as a function of time.

3. Testing of models

We now have a realization of an isotropic turbulent flow. The velocities and pressure are available at $(64)^3$ grid points at 50 times. This contrasts with experimental data that contain many time points but relatively little spatial resolution. The computed flow can then be used as input for the analysis of various models of the subgrid-scale turbulence.

Consider again (1) and (2). Leonard (1973) has suggested that the appropriate averaging process for large eddy simulation should be a local spatial average:

$$\overline{u}_i(\mathbf{x}) = \int G(\mathbf{x}-\mathbf{x}')\,u_i(\mathbf{x}')\,d\mathbf{x}', \tag{13}$$

where G is a normalized weighting function as yet unspecified. This process may be called filtering, as its effect is to remove the small-scale fluctuations from u_i in forming $\overline{u}_i$ the filtered or large-scale field and u_i' (defined below) the subgrid-scale field.

A simple choice is to let $G = 1$ within a cubic volume with sides of length Δ_a centred at x and let $G = 0$ outside. Then

$$\overline{u}_i(\mathbf{x}) = \frac{1}{\Delta_a^3}\int\int\int u_i(x_1 - x_1', x_2 - x_2', x_3 - x_3')\, dx_1' dx_2' dx_3', \tag{14}$$

the integrations being from $x_1 - \frac{1}{2}\Delta_a$ to $x_1 + \frac{1}{2}\Delta_a$, $x_2 - \frac{1}{2}\Delta_a$ to $x_2 + \frac{1}{2}\Delta_a$ and from $x_3 - \frac{1}{2}\Delta_a$ to $x_3 + \frac{1}{2}\Delta_a$.

We now obtain the filtered counterparts of (1) and (2) by multiplying each by the weighting function $G = 1$ and integrating over the cubic volume V to obtain

$$\frac{\partial \overline{u}_i}{\partial t} + \frac{\partial}{\partial x_j}\overline{u_i u_j} = -\frac{\partial \overline{p}}{\partial x_i} + \nu \nabla^2 \overline{u}_i, \tag{15}$$

$$\partial \overline{u}_i / \partial x_i = 0. \tag{16}$$

We now make the substitution $u_i = \overline{u}_i + u_i'$ in the nonlinear advective term and obtain

$$\frac{\partial t}{\partial \overline{u}_i} + \frac{\partial}{\partial x_j}\overline{\overline{u}_i \overline{u}_j} = -\frac{\partial \overline{p}}{\partial x_i} + \nu \nabla^2 \overline{u}_i - \frac{\partial}{\partial x_j}\eta_{ij}, \tag{17}$$

where

$$\eta_{ij} = \overline{\overline{u}_i \overline{u}_j'} + \overline{u_i' \overline{u}_j} + \overline{u_i' u_j'} \tag{18}$$

is the subgrid-scale counterpart of the Reynolds stress.

We stress the fact that (17) is exact. We have defined new variables, but so far we have made no approximations. Also $\overline{u}_i$ and u_i' are continuous variables defined at all points in space and time, and are in no way tied to a finite grid of points.

In order to solve (17) it is now necessary to make some approximations. The testing of these approximations is the purpose of our main numerical simulation. Commonly used approximations are (cf. Deardorff 1970)

$$\overline{\overline{u}_i \overline{u}_j} \simeq \overline{u}_i \overline{u}_j, \tag{19}$$

$$\overline{\overline{u}_i u_j'} + \overline{u_i' \overline{u}_j} \simeq 0, \tag{20}$$

$$\tau_{ij} + \overline{u_i' u_j'} = f(\overline{u}_i, \overline{u}_j). \tag{21}$$

The major purpose of this paper is to investigate these approximations, test their validity, and suggest improvements. Alternatively, one can include $\overline{\overline{u}_i \overline{u}_j} - \overline{u}_i \overline{u}_j$ and the left-hand side of (20) in the definition of τ_{ij} and regard the model as one for the combination so obtained. We have not tested this possibility.

Leonard (1973) has shown that (19) is probably a poor approximation in turbulent flow and has derived a model for the associated error. Clark *et al.* (1977) have shown that (20) is a poor approximation and have derived a model for the error.

We now imagine placing a coarse $8 \times 8 \times 8$ mesh over the physical space occupied by the fine mesh used in computing the flow field. Thus each side of the coarse mesh is eight times a side of the original fine mesh. This mesh can be thought of as the one we might use in a large eddy simulation of this flow. The relation between the meshes is illustrated in figure 6. Within each cell of the coarse mesh, we have the velocity

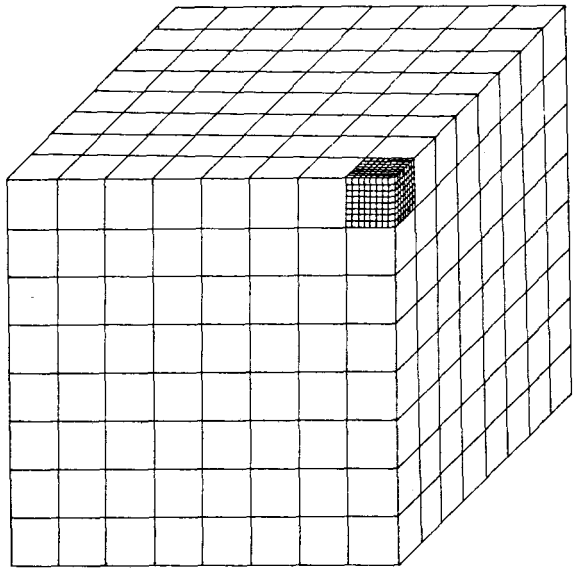

FIGURE 6. Illustration of fine mesh inside coarse mesh.

field $\overline{u}_i$ at 512 evenly spaced points. Now we need to compute the filtered velocity field $\overline{u}_i$ at each point in the fine mesh. We actually used the box filter (14) with sides of length $\Delta_a = \frac{17}{8}\Delta$, where Δ is the mesh spacing of the coarse grid, rather than 2Δ, so that the fine mesh points are evenly distributed on both sides of the point at which we want the average. The filtered velocity $\overline{u}_l(i,j,k)$, where i,j,k are the co-ordinates of the point on the fine grid, is

$$\overline{u}_l(i,j,k) = \frac{1}{17^3} \sum_{i'=i-8}^{i+8} \sum_{j'=j-8}^{j+8} \sum_{k'=k-8}^{k+8} u_l(i',j',k'). \tag{22}$$

Calculations will also be made using an averaging volume with side $\frac{9}{8}\Delta$. Having calculated $\overline{u}_l$, we also have u'_l from its definition $u_l - \overline{u}_l = u'_l$. For illustration purposes we have randomly chosen a line of 64 points in the x_1 direction and have plotted $u_1(x_1)$ and $\overline{u}_1(x_i)$ for these 64 points in figure 7.

The remaining quantities in which we are interested are computed from

$$\overline{\overline{u}_l \overline{u}_m} = \frac{1}{17^3} \sum_{i'} \sum_{j'} \sum_{k'} \overline{u}_l \overline{u}_m, \tag{23}$$

$$\overline{\overline{u}_l u'_m} = \frac{1}{17^3} \sum_{i'} \sum_{j'} \sum_{k'} \overline{u}_l u'_m, \tag{24}$$

$$\overline{u'_l u'_m} = \frac{1}{17^3} \sum_{i'} \sum_{j'} \sum_{k'} u'_l u'_m. \tag{25}$$

We now restrict our attention to the quantities $\overline{u}_i$, $\overline{\overline{u}_i \overline{u}_j}$, $\overline{\overline{u}_i \overline{u}_i}$ and $\overline{u'_i u'_j}$ at the centres of the 512 cells defined by the coarse mesh. The claim made for the models under investigation is that the variables $\overline{\overline{u}_i \overline{u}_j}$, $\overline{\overline{u}_i u'_j}$ and $\overline{u'_i u'_j}$ can be expressed as functionals of $\overline{u}_i$. We shall now demonstrate the extent to which this is true for the particular flow field we have simulated.

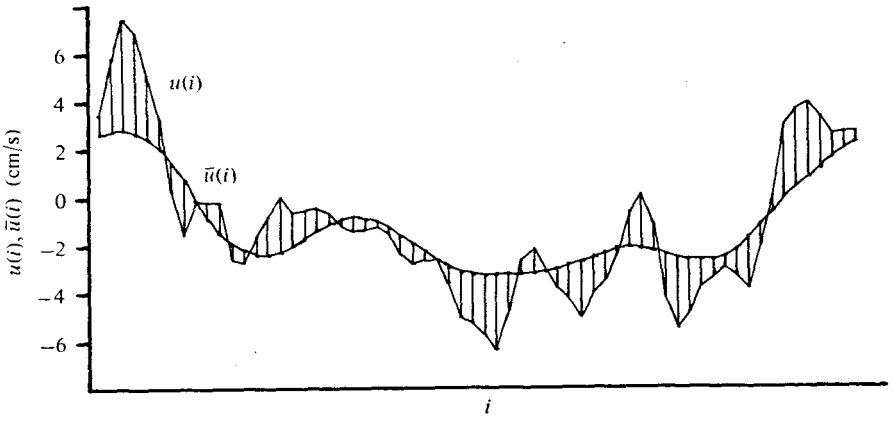

FIGURE 7. Sample of filtered and unfiltered velocity fields.

We can compare the models for subgrid-scale turbulence terms with their numerical experimental values. We define the conventional correlation coefficient $C(M, X)$ between the prediction of the model M and the exact experimental value X by

$$C(M, X) = \langle MX \rangle / \langle M^2 \rangle^{\frac{1}{2}} \langle X^2 \rangle^{\frac{1}{2}}, \tag{26}$$

where

$$\langle MX \rangle = \frac{1}{512} \sum_{n=1}^{512} M(n) X(n), \tag{27}$$

$$\langle M^2 \rangle = \frac{1}{512} \sum_{n=1}^{512} M^2(n), \tag{28}$$

$$\langle X^2 \rangle = \frac{1}{512} \sum_{n=1}^{512} X^2(n). \tag{29}$$

If M and X are totally unrelated, then $C(M, X) = 0$. If M is a constant multiple of X, i.e. if the model is exact, $C(M, X) = 1$.

There are three levels at which comparisons can be made. For the moment we restrict the discussion to the subgrid-scale Reynolds stress τ_{ij}. The most direct comparison is at the tensor level, i.e. between the experimental and modelled components τ_{ij}. On the other hand, the term which actually occurs in the momentum equation is an acceleration vector $\partial \tau_{ij}/\partial x_j$. We define the vector level of comparison to be that between the experimental and modelled values of $\partial \tau_{ij}/\partial x_j$. The scalar level of comparison refers to the energy dissipation $\bar{u}_i \partial \tau_{ij}/\partial x_j$ in each cell of the coarse mesh by the experimental and modelled τ_{ij}. As the primary purpose of the subgrid-scale model is to remove kinetic energy at the correct locations in the flow, the scalar level of comparison is quite significant.

Tensor-level comparisons

The Leonard term. The Leonard term is defined as

$$L_{ij} = \Lambda_{ij} - \tfrac{1}{3}\Lambda_{kk}\delta_{ij}, \quad \Lambda_{ij} = \overline{\bar{u}_i \bar{u}_j} - \bar{u}_i \bar{u}_j, \tag{30a}$$

and the model we use for L_{ij} (Leonard 1973) is

$$M_{ij} = \alpha_{ij} - \tfrac{1}{3}\alpha_{kk}\delta_{ij}, \quad \alpha_{ij} = \tfrac{1}{24}\Delta_a^2 \nabla^2(\bar{u}_i \bar{u}_j), \tag{30b}$$

where Δ_a is the size of the averaging box ($\frac{9}{8}\Delta$ or $\frac{17}{8}\Delta$). Fourth-order differencing has been used in evaluating all of the models. Fourth-order space differencing was found to give 1–3 % better correlations than second-order differencing. The differencing was done on the coarse mesh, because this is the mesh which would be used in a modelled simulation. Since we have $\overline{u}_i$ on the fine mesh as well as on the coarse mesh, we can get more accurate approximations to the derivatives. We compared the results obtained by differencing on the fine mesh with those obtained on the coarse mesh and found the differences to be small (the correlations for the Leonard, cross and Reynolds terms in the case of the $\frac{9}{8}\Delta$ filter changed from 0·909, 0·790 and 0·277 to 0·934, 0·744 and 0·297, respectively).

The correlation between the model (31) and the experiment (30) is 0·935 for the large ($\frac{17}{8}\Delta$) filter and 0·909 for the small ($\frac{9}{8}\Delta$) filter. The ratio of the r.m.s. value from the model to the r.m.s. value from the experiment is 1·60 for the large filter and 0·788 for the small filter; this ratio represents the proportionality constant of the model and the reason why these values differ from each other and from the expected value of unity (Leonard 1973) are not understood. Since the model for the Leonard term is based on the fewest approximations among the three terms we are considering, we expect it to be the best, which it is. Also, since the model is based on a Taylor series expansion of the filtered velocity field, we expect the smoother velocity field produced by the larger filter to give better results, and it does.

The cross-term. The cross-term is defined as

$$C_{ij} = \kappa_{ij} - \tfrac{1}{3}\kappa_{kk}\delta_{ij}, \quad \kappa_{ij} = \overline{\overline{u}_i\overline{u}_j} + \overline{u'_i\overline{u}_j}, \tag{31a}$$

and the model used for C_{ij} is

$$M_{ij} = \alpha_{ij} - \tfrac{1}{3}\alpha_{kk}\delta_{ij}, \quad \alpha_{ij} = -\tfrac{1}{24}\Delta_a^2(\overline{u}_i\nabla^2\overline{u}_j + \overline{u}_j\nabla^2\overline{u}_i). \tag{31b}$$

For its derivation, see Clark *et al.* (1977). In this case, the correlation is better for the small filter than for the large filter. This is probably because the experimental values are smaller for the large filter than for the small filter, owing to the smoother flow field. The correlations of 0·685 and 0·790 are less than for the Leonard term, but the r.m.s. ratios of model to experiment are both closer to each other and to unity; they are 1·23 and 0·96 for the large and small filters, respectively.

The subgrid-scale Reynolds stress. The definition of the subgrid-scale Reynolds stress is

$$\tau_{ij} = \sigma_{ij} - \tfrac{1}{3}\sigma_{kk}\delta_{ij}, \quad \sigma_{ij} = \overline{u'_iu'_j}. \tag{32}$$

The four models we shall consider are all of the eddy-viscosity type, i.e.

$$M_{ij} = \alpha_{ij} - \tfrac{1}{3}\alpha_{kk}\delta_{ij}, \quad \alpha_{ij} = K\left(\frac{\partial\overline{u}_i}{\partial x_j} + \frac{\partial\overline{u}_j}{\partial x_i}\right), \tag{33}$$

where K is given by

$$K = (C\Delta_a)^2\left[\frac{1}{2}\left(\frac{\partial\overline{u}_i}{\partial x_j} + \frac{\partial\overline{u}_j}{\partial x_i}\right)\left(\frac{\partial\overline{u}_i}{\partial x_j} + \frac{\partial\overline{u}_j}{\partial x_i}\right)\right]^{\frac{1}{2}} \quad \text{for model 1 (Smagorinsky 1963),} \tag{34}$$

$$K = (C\Delta_a)^2(\overline{\omega}_i\overline{\omega}_i)^{\frac{1}{2}} \quad \text{for model 2 (vorticity),} \tag{35}$$

$$K = \tfrac{1}{3}(C\Delta_a)(\overline{u'_ku'_k})^{\frac{1}{2}} \quad \text{for model 3 (turbulent kinetic energy),} \tag{36}$$

$$K = C \quad \text{for model 4 (constant eddy viscosity).} \tag{37}$$

In (35), ω_i represents the vorticity $\omega_i = \epsilon_{ijk}(\partial u_k/\partial x_j)$. In model 3, the value for $\overline{u'_k u'_k}$ is taken from the experimental data. The values obtained are given in table 2. All four models were found to be approximately equally valid with the best correlations found to be 0·363 for the large filter and 0·303 for the small filter. Although these correlations are considerably below those for the cross and Leonard terms, they are clearly significant. The constants in the models were obtained by matching the r.m.s. value of the exact quantity with that of the model prediction.

Vector-level comparison

The Leonard and cross terms. In the previous section, we compared the models directly with the corresponding stress tensors. Here we make the comparison with the terms which actually enter the momentum equations, i.e. $\partial L_{ij}/\partial x_j$ and $\partial C_{ij}/\partial x_j$. The results for the large filter show that the correlations range from 0·935 to 0·947 for the Leonard term and from 0·685 to 0·689 for the cross term for the three components. For all practical purposes these are the same as for the tensor-level comparison.

The subgrid-scale Reynolds stress. In contrast to the case for the Leonard and cross terms, we find a significant increase in the correlations between the model prediction of $\partial \tau_{ij}/\partial x_j$ and its experimental value over the correlation at the tensor level. The results shown in table 2 show that all models are again equally good, but the correlation has typically increased from 0·35 to 0·42 for the large filter. Comparable increases are seen in the results for the small filter. The reason for this increase is not understood. We note also that, with one exception, the model constants decrease.

Scalar-level comparison

The Leonard and cross terms. Here we base our comparisons on the terms which enter the energy equation, i.e. $\bar{u}_i \partial L_{ij}/\partial x_j$ and $\bar{u}_i \partial C_{ij}/\partial x_j$. We find a small decrease in the correlations in going from the vector to the scalar level for both Leonard and cross terms. There is a large relative disagreement between the values of the dissipation due to the Leonard term at the two filter widths. This is not serious, since the dissipation due to the Leonard term is itself relatively small.

The subgrid-scale Reynolds stress. We find a very sharp increase in the correlations for the subgrid-scale Reynolds stress at the scalar level. For example, at the vector level, the Smagorinsky model with $\Delta_a = \frac{17}{8}\Delta$ had a correlation of 0·425, but at the scalar level it is 0·710. Part of the increase may be due to the fact that both the experimental and the modelled terms have mean values which are significantly positive. Even so, when the mean values of both are subtracted out, the correlation between the fluctuating components of the exact and model values is still 0·535. We also note a further decrease in the model constant.

The subgrid-scale eddy coefficient

The models contain constants, which are usually called the subgrid-scale eddy coefficient. The value of the constant has no effect on the correlation between model and experiment. As mentioned above, we can adjust the constant to match the r.m.s. values of the model and experiment. The values of the constants found in this way are given in table 2 and were mentioned earlier. The constants obtained decrease as we pass from the tensor level of comparison to the scalar level. Since the primary

Term	Model	Correlation $\frac{17}{8}\Delta$	Correlation $\frac{9}{8}\Delta$	Model constant $\frac{17}{8}\Delta$	Model constant $\frac{9}{8}\Delta$
τ_{ij}	Smagorinsky	0·366	0·277	0·270	0·247
(tensor)	Vorticity	0·344	0·260	0·294	0·275
	Turbulent kinetic energy	0·363	0·303	0·196	0·175
	Eddy viscosity	0·352	0·295		
$\frac{\partial \tau_{ij}}{\partial x_j}$	Smagorinsky	0·425	0·346	0·240	0·264
	Vorticity	0·408	0·327	0·220	0·247
(vector)	Turbulent kinetic energy	0·434	0·362	0·138	0·155
	Eddy viscosity	0·426	0·356		
$u_i \frac{\partial \tau_{ij}}{\partial x_j}$	Smagorinsky	0·710	0·580	0·186	0·171
	Vorticity	0·700	0·582	0·202	0·191
(scalar)	Turbulent kinetic energy	0·723	0·606	0·085	0·095
	Eddy viscosity	0·716	0·605		

TABLE 2. Summary of correlations between exact subgrid-scale Reynolds stresses and models.

function of these models is to represent the transfer of energy from large to small scales, which acts like a dissipation to the large scales, we recommend that the values given for the scalar level of comparison be used. For the Smagorinsky model, these values are in excellent agreement with theoretical and experimental values, which range from around 0·13 to 0·21 (Deardorff 1971; Mansour *et al.* 1977). We note that when the Smagorinsky model is written using the term $(C\Delta_a)^2$ the value of C is nearly independent of Δ_a; this would not be the case if the finite-difference grid spacing Δ were used. It is encouraging that we have obtained about the same value for C as is obtained by theoretical arguments assuming an inertial subrange and by numerical experiments at higher Reynolds numbers. This leads us to speculate that C is nearly independent of the spectrum of turbulence and Reynolds number, at least in the isotropic case for Reynolds numbers above the ones used here. (Note that the proper Reynolds number in this connexion is the subgrid-scale Reynolds number $u'\Delta/\nu$, not the quantity Re_λ introduced earlier. These numbers are of the same order of magnitude, however.) The values we obtain are within 10% of those found by Kwak *et al.* (1975), Shaanan, Ferziger & Reynolds (1975) and Mansour *et al.* (1977) by matching model calculations to experimental energy decay. Since a change in numerical method can result in a 10% change in the constant, we can say that we have indeed *predicted* the model constant without reference to experiment.

Comments on the correlations

A striking result is that all four of the models are essentially equally valid. Since all of the models use a positive scalar times $\partial\bar{u}_i/\partial x_j + \partial\bar{u}_j/\partial x_i$, we checked to see how often the sign of τ_{ij} coincided with the sign of $\partial\bar{u}_i/\partial x_j + \partial\bar{u}_j/\partial x_i$ and found it to be only 68%. We also ran a calculation with K adjusted at each point in space so as to give the best possible correlation. At the tensor level of comparison, we achieved a correlation of 0·51 *vs.* 0·35 for the models considered above. We conclude that no model of the form (33) can do very much better than Smagorinsky's. This includes models

which attempt to calculate the transport of turbulent kinetic energy and models which attempt to calculate both the turbulent kinetic energy and a length scale or the dissipation (so called two-equation models). This is partially verified by the results of model (36), which show that, even if one could calculate exactly the turbulent kinetic energy in each cell, this would not give a significant improvement. Also, note that the constant in the eddy-viscosity model (37) is dimensional, so that this model is not really a serious contender as the constant would need to be adjusted for each flow; it was included merely to show how a simple model might perform. Some possible exceptions will be noted in § 4 below.

Other models, which were discarded

The models considered above are reasonably good. We list here some of the more reasonable-looking models which were tried but discarded. The following three-tensor eddy viscosity models all had correlations of less than 0·02 with the numerical experiment:

$$\tau_{ij} = C\Delta_a^2 D_{ik} D_{kj},$$

$$\tau_{ij} = \tfrac{1}{2} C\Delta_a^2 (R_{ik} D_{kj} + R_{jk} D_{ki}),$$

$$\tau_{ij} = \tfrac{1}{2} C\Delta_a^2 (D_{ik} D_{kj} + R_{jk} R_{kj}),$$

where D_{ij} is the strain-rate tensor

$$D_{ij} = \tfrac{1}{2}(\partial \bar{u}_i/\partial x_j + \partial \bar{u}_j/\partial x_i),$$

and R_{ij} is the rotation tensor

$$R_{ij} = \tfrac{1}{2}(\partial \bar{u}_i/\partial x_j - \partial \bar{u}_j/\partial x_i).$$

The next three models are similar to the Leonard term, and all had correlations with τ_{ij} of less than 0·02:

$$\tau_{ij} = \frac{\partial}{\partial x_k}\frac{\partial}{\partial x_k}\bar{u}_i \bar{u}_j,$$

$$\tau_{ij} = \frac{\partial}{\partial x_i}\frac{\partial}{\partial x_j}\bar{u}_k \bar{u}_k,$$

$$\tau_{ij} = \frac{1}{2}\left[\frac{\partial}{\partial x_i}\frac{\partial}{\partial x_k}(\bar{u}_j \bar{u}_k) + \frac{\partial}{\partial x_j}\frac{\partial}{\partial x_k}(\bar{u}_i \bar{u}_k)\right].$$

We are continuing to investigate still other models and the results will be reported in the future.

4. Discussion and conclusion

We have shown that it is possible to simulate homogeneous isotropic turbulence at low Reynolds numbers. Present computational capacity restricts the range of Reynolds number based on the Taylor microscale to less than about 40. New computers (such as the Cray I) will allow an increase in the Reynolds number of a factor of two or, perhaps, four. The scaling is such that the use of exact simulation will be restricted to relatively simple flows for some time to come. We therefore expect that

the major application of exact simulations of turbulent flows will be in the testing of models along the lines of this paper and in the testing of theories as others have done.

It must be emphasized again that the results obtained in this paper apply only to the particular flow treated here and caution is necessary in drawing any sweeping conclusions. It is likely that some of the results apply to a wider range of flows than the one treated here and some speculations will be made below. These must, however, be considered for what they are.

The modelling suggested by Leonard for the term $\overline{\overline{u}_i\overline{u}_j}-\overline{u}_i\overline{u}_j$ has been found to be of acceptable accuracy but the fact that the constant appears to depend on the averaging width is an unexpected result, and no explanation for it has yet been found. This is a subject that requires further investigation. An alternative is to compute the term $\overline{\overline{u}_i\overline{u}_j}$ directly (Mansour *et al.* 1977). We expect the importance of this term to be nearly Reynolds number independent.

The modelling of the cross term $\overline{u_i'\overline{u}_j}+\overline{\overline{u}_i u_j'}$ is also quite good. The importance of this term should decrease with increasing Reynolds number. This term can also be combined with the Leonard term to give a simpler combined model that ought to be both simple to compute and quite accurate.

The modelling of the subgrid-scale Reynolds stress is not so good as to eliminate the need for improvements, but neither is it so bad as to cause one to reject it out of hand; we were unable to find any model more accurate than Smagorinsky's. It is encouraging that the model constant can be adequately predicted without reference to experimental data. Since the value of the constant that we obtained at relatively low Reynolds number is very close to the one found from both high Reynolds number theories and our earlier modelled simulations at higher Reynolds numbers, it appears that the constant is independent of Reynolds number, at least above the one we have used. Again, the proper Reynolds number is the one based on subgrid-scale parameters and is approximately equal to Re_λ. We are currently investigating lower Reynolds numbers, and it appears that the viscous effects that are expected theoretically indeed appear and that modification of the model will be necessary. It thus appears safe to conclude that, so long as the subgrid-scale turbulence is nearly isotropic and its Reynolds number is high enough, the models of eddy-viscosity type are sufficiently accurate for most purposes.

The inaccuracy of the model seems to arise more from the fact that the subgrid-scale Reynolds stress tensor and the large-scale strain-rate tensor have principal axes that are not aligned than from the inaccurate representation of the eddy viscosity. This means that, except in transitional flows as noted in the previous paragraph, the use of one- and two-equation subgrid-scale models is not likely to provide a significant improvement over the simple Smagorinsky model used here. There may be implications in this for Reynolds-stress modelling, but any conclusions of this nature would be very speculative at present.

One case in which modification to the model is certain to be required is that of developing and transitional flows. In these cases, the large-scale turbulence must be allowed to develop before any subgrid-scale turbulence can appear, and the relationship between the subgrid turbulence and the resolvable field is quite different from that assumed in deriving the models. Use of the subgrid-scale models at too early a time in such flows may simply prevent transition from occurring, and we shall surely

need a model that allows the subgrid-scale effects to lag behind the resolvable field turbulence.

Many extensions of this work are possible, and some are currently being carried out and will be reported at a later time. Among the lines of investigation will be the search for more accurate representation of the subgrid-scale Reynolds-stress tensor by means of other tensors. Higher-level models, lower Reynolds numbers, and the effects of anisotropy and large-scale strain are among the topics currently being considered.

This paper is based in part on a dissertation submitted by one of the authors (R. A. Clark) in partial fulfilment of the requirements for the PhD. at Stanford University. The work was done under a grant from NASA-Ames Research Center (NgR-020-05-622). The authors gratefully acknowledge conversations with Dr A. Leonard, Dr D. Kwak, Dr S. Shaanan, Dr U. Mehta, Dr N. Mansour and Dr P. Moin.

REFERENCES

Batchelor, G. K. 1953 *The Theory of Homogeneous Turbulence.* Cambridge University Press.

Clark, R. A., Ferziger, J. H. & Reynolds, W. C. 1977 Evaluation of subgrid-scale turbulence models using a fully simulated turbulent flow. *Mech. Engng Dept., Stanford Univ. Rep.* TF-9.

Comte-Bellot, G. & Corrsin, S. 1971 Simple Eulerian time correlation of full- and narrow-band velocity signals in grid-generated 'isotropic' turbulence. *J. Fluid Mech.* **48**, 273.

Deardorff, J. W. 1970 A numerical study of three dimensional turbulent flow at large Reynolds numbers. *J. Fluid Mech.* **41**, 453.

Deardorff, J. W. 1971 On the magnitude of the subgrid scale eddy coefficient. *J. Comp. Phys.* **7**, 120.

Kwak, D., Reynolds, W. C. & Ferziger, J. H. 1975 Three dimensional time dependent computation of turbulent flows. *Mech. Engng Dept., Stanford Univ. Rep.* TF-5.

Leonard, A. 1973 On the Energy Cascade in Large-Eddy Simulations of Turbulent Flows. *Adv. in Geophys.* **A18**, 237.

Mansour, N. N., Moin, P., Reynolds, W. C. & Ferziger, J. H. 1977 Improved methods for large-eddy simulation of turbulence. *Proc. Penn State Symp. Turbulent Shear Flows.*

Orszag, S. A. & Patterson, G. S. 1972 Numerical Simulation of three dimensional homogeneous isotropic turbulence. *Phys. Rev. Lett.* **28**, 76.

Rogallo, R. 1977 An ILLIAC program for the numerical simulation of homogeneous incompressible turbulence. *N.A.S.A. Tech. Memo.* no. 73, 203.

Shaanan, S., Ferziger, J. H. & Reynolds, W. C. 1975 Numerical simulation of turbulence in the presence of shear. *Mech. Engng Dept., Stanford Univ. Rep.* TF-6.

Smagorinsky, J. 1963 General circulation experiments with the primitive equations. *Mon. Weath. Rev.* **93**, 99.

Van Atta, C. W. & Chen, W. Y. 1969 Measurements of spectral energy transfer in grid turbulence. *J. Fluid Mech.* **38**, 743.